HHS Public Access

Author manuscript

Mucosal Immunol. Author manuscript; available in PMC 2022 February 05.

Published in final edited form as:

Mucosal Immunol. 2021 November ; 14(6): 1369–1380. doi:10.1038/s41385-021-00436-0.

Deficient inflammasome activation permits an exaggerated asthma phenotype in rhinovirus C-infected immature mice

Mingyuan Han, PhD[1], **Tomoko Ishikawa, MS**[1], **Claudia C. Stroupe, BA**[1], **Haley A. Breckenridge, BA**[1], **J. Kelley Bentley, PhD**[1], **Marc B. Hershenson, MD**[1,2]

[1]Department of Pediatrics, University of Michigan Medical School, Ann Arbor, MI 48109

[2]Department of Molecular and Integrative Physiology, University of Michigan Medical School, Ann Arbor, MI 48109

Abstract

Compared to other RV species, RV-C has been associated with more severe respiratory illness and is more likely to occur in children with a history of asthma or who develop asthma. We therefore inoculated six-day-old mice with sham, RV-A1B, or RV-C15. Inflammasome priming and activation were assessed, and selected mice treated with recombinant IL-1β. Compared to RV-A1B infection, RV-C15 infection induced an exaggerated asthma phenotype, with increased mRNA expression of *Il5, Il13, Il25, Il33, Muc5ac, Muc5b* and *Clca1,* increased lung lineage-negative CD25+CD127+ST2+ ILC2s, increased mucous metaplasia, and increased airway responsiveness. Lung vRNA, induction of pro-inflammatory type 1 cytokines, and inflammasome priming (pro-IL-1β and NLRP3) were not different between the two viruses. However, inflammasome activation (mature IL-1β and caspase-1 p12) was reduced in RV-C15-infected mice compared to RV-A1B-infected mice. A similar deficiency was found in cultured macrophages. Finally, IL-1β treatment decreased RV-C-induced type 2 cytokine and mucus-related gene expression, ILC2s, mucous metaplasia and airway responsiveness, but not lung vRNA level. We conclude that RV-C induces an enhanced asthma phenotype in immature mice. Compared to RV-A, RV-C-induced macrophage inflammasome activation and IL-1β are deficient, permitting exaggerated type 2 inflammation and mucous metaplasia.

Keywords

asthma; IL-1β; IL-25; IL-33; type 2 innate lymphoid cell

Corresponding author: Marc B. Hershenson, Medical Sciences Research Building II, 1150 W. Medical Center Drive, Ann Arbor, MI; Phone, 734-936-4200; Fax, 734-764-3200; mhershen@umich.edu.

Author Contributions:

Study design: M.H. and M.B.H.; data collection: M.H., T.I., C.C.S. H.A.B. and J.K.B.; analysis: M.H. and M.B.H.; manuscript drafting and editing: M.H., J.K.B. and M.B.H.; manuscript approval—all authors.

Conflict of Interest Statement: No conflict

Introduction

Human rhinoviruses (RVs) are positive-strand RNA viruses grouped in the genus *Enterovirus* in the family *Picornaviridae*. In addition to the previously-discovered species RV-A and RV-B, a new species RV-C was firstly identified by highly-sensitive genome sequencing for a variety of clinical specimens in 2006 [1, 2].Thus far, 55 RV-C genotypes have been reported [3, 4]. Intercellular adhesion molecule 1 (ICAM-1) and low-density lipoprotein receptor (LDLR) [5, 6], receptors for major and minor RV-A and RV-B subtypes, are expressed on airway epithelial cells[7, 8] and immune cells such as macrophages[9, 10], mast cells, and basophils[11, 12]. RV-C infection is restricted to ciliated airway epithelial cells that express the RV-C receptor cadherin related family member 3 (CDHR3) [13–15].

Accumulating evidence indicates that RV-C is the most prevalent rhinovirus species detected in children diagnosed with acute respiratory illness. Infections with RV-C are more likely to occur in children with a history of asthma or who develop asthma [16–21]. In a prospective study of children less than 5 years of age from two U.S. counties, children with RV-C infections were significantly more likely than those with RV-A infections to have underlying high-risk conditions such as asthma (42% vs 23%) and to have a discharge diagnosis of asthma (55% vs 36%)[16]. In addition, in a prospective study of 260 children hospitalized in the pediatric intensive care unit with a diagnosis of either acute asthma exacerbation or bronchiolitis, RV-C was present in 22.3% of samples, followed by RV-A (17.5%) and RV-B (1.7%) [21]. Finally, recent data suggest a possible role for early-life RV-C infections in asthma development. A multicenter prospective study of U.S. infants hospitalized for bronchiolitis found that only infants with RV-C had a higher risk of physician-diagnosed asthma at 4 years of age [22]. Allergic sensitization was additive but not necessary for asthma development. These investigators also found that severe RV bronchiolitis was associated with greater nasopharyngeal type 2 cytokine levels [23].

Epidemiologic studies in high-risk infants indicate that early-life wheezing-associated respiratory infection with RV is a major predisposing factor for asthma development[24–27]. We have shown that RV-A1B infection of 6-day-old immature mice causes the development of a chronic asthma-like mucous metaplasia phenotype which requires expansion of IL-13-producing type 2 innate lymphoid cells (ILC2s)[28, 29]. RV-induced innate cytokines IL-25, IL-33 and TSLP work cooperatively for maximal ILC2s expansion and function [30]. Further, we found that RV-A1B triggered Nod-like receptor protein 3 (NLRP3) inflammasome activation and IL-1β production in the airway macrophages of 6-day old mice[31]. Macrophage IL-1β limited type 2 inflammation and mucous metaplasia following RV-A1B infection by suppressing production of the epithelial cell innate cytokines and ILC2 function.

No experimental studies have investigated the association of early-life RV-C infection in asthma development. To address this knowledge gap, we infected six-day-old immature mice with RV-C15 and compared the asthma phenotypes with RV-A1B infected mice. We hypothesize that RV-C causes an exaggerated asthma phenotype which is permitted in part by reduced inflammasome activation.

Results

RV-C15 infection of six-day old mice.

cDNA encoding RV-C15 and HeLa-E8 cells expressing CDHR3 C529Y were provided by James Gern and Yury Bochkov, University of Wisconsin.[14] Six day-old C57BL/6J mice were inoculated intranasally with 1.5×10^6 PFU equivalents (ePFU) of RV-C15 in 15 μL PBS, 1.5×10^6 ePFU RV-A1B or an equal volume of sham HeLa cell lysate. There was no difference in lung viral load 1, 4, and 7 days post-infection (Fig 1A). Two days after infection, RV-C15 significantly induced *Ifna* mRNA expression (Fig. 1B). Lungs were also formalin-fixed and paraffin-embedded two days after exposure and sections stained with fluorescent tagged anti-enterovirus viral protein 3 (vp3), acetyl-α-tubulin and anti-CDHR3. RV-C15 but not RV-A1B colocalized with CDHR3 in ciliated airway epithelial cells (Fig 1C). We also found RV-C15 in airway CD11b+ macrophages.

RV-C15 causes an exaggerated asthma-like phenotype in immature mice.

RV-A1B infection of six-day old immature mice induces an asthma-like phenotype and type 2 inflammatory responses [28, 32]. To examine virus species differences, we infected 6-day-old mice with sham HeLa cell lysate, RV-A1B and RV-C15. Again, early-life RV-A1B infection induced a mucous metaplasia phenotype, as evidenced by periodic acid–Schiff (PAS) staining and Muc5ac protein deposition in the airway epithelium 21 days after infection (Fig. 2A and 2B). RV-A1B infection also increased mRNA levels of type 2 cytokines *Il5* and *Il13* and mucus-related genes *Muc5ac, Muc5b, and Clca1* (Fig. 2C). In addition, compared to sham infection, RV-A1B infection increased airway responsiveness to methacholine (Fig. 2E).

We then examined the response of six-day-old mice to RV-C15. Compared to RV-A1B, RV-C15 infection of 6-day old mice induced significantly higher mRNA expression of *Il5* and *Il13* as well as the mucus-related genes *Muc5ac, Muc5b* and *Clca1.* RV-C also caused even greater PAS staining, Muc5ac protein accumulation and airway responsiveness compared to RV-A. In contrast, compared to sham treatment, both RV-A1B and RV-C significantly increased mRNA expression of the type 1 cytokines *Tnf, Ifng*, *Cxcl1,* and *Cxcl2* (Fig. 2D). There was no difference in *Tnf, Ifng., Cxcl1* or *Cxcl2* mRNA expression between RV-A1B and RV-C15. RV-C15 did not increase *Il17* mRNA.

We previously reported that ILC2s are indispensable for the early-life RV infection-induced type 2 cytokine production and mucous metaplasia[28, 29]. We compared lung ILC2s in RV-A1B and RV-C15 infected immature mice. Seven days after infection, RV-A1B significantly expanded lineage negative, CD25-positive, CD127-positive, and ST2-positive ILC2s as reported previously (Fig 3A). Compared to RV-A1B, RV-C15 further increased the number of lung ILC2s. Compared to RV-A infection, ILCs were significantly higher after RV-C infection four and seven days post-inoculation (Fig 3B). Higher ILC2 numbers in RV-C15-infected mice were observed as early as four days after infection and maintained two weeks after infection. These results are consistent with the notion that early-life infection of RV-C15 exaggerates the development of the asthma phenotype via regulation ILC2 expansion.

Comparison of RV-C15- and RV-A1B-induced innate cytokines.

The innate cytokines IL-25, IL-33, and TSLP cooperate to promote ILC2 function and expansion during early-life RV infection[30]. We therefore compared lung innate cytokine responses to RV-C15 and RV-A1B. IL-33, IL-25, and TSLP mRNA and protein expression were induced by RV-A1B infection. mRNA and protein levels of IL-33 were measured day 1 after infection and IL-25 and TSLP were measured 7 days after infection (Fig 4A, 4B), when their production is maximal[30, 31]. Cytokine deposition was also detected by immunofluorescence microscopy two days after infection (Fig 4C). Relative to RV-A1B, innate cytokine expression was significantly increased in the RV-C15-infected mice.

RV-C15-induced inflammasome activation is deficient in cultured macrophages.

We have shown that RV-A1B infection induces macrophage inflammasome priming and activation in both mature [33] and immature mice [31]. Inflammasome priming (step 1), as evidenced by mRNA and protein abundance of pro-IL-1β and NLRP3, is dependent on TLR2 whereas inflammasome activation (step 2), as demonstrated by protein abundance of mature IL-1β and caspase-1 p12, is dependent on viral genome [33]. While inflammasome priming is reduced in immature compared to mature mice, IL-1β tends to limit the asthma phenotype by attenuating RV-induced airway innate cytokine responses [31]. We reasoned that, in immature mice, deficient inflammasome activation by RV-C15 might permit an even higher level of innate cytokine expression and ILC2 expansion, leading to an exaggerated asthma phenotype. We therefore examined viral-induced inflammasome activation in cultured macrophages. RV-A1B and RV-C15 induced equal expression of pro-IL-1β and NLRP3 in human PBMC-derived macrophages, THP-1-derived macrophages, and mouse bone marrow-derived macrophages (Figs 5A–5C). TLR2−/− bone marrow-derived macrophages showed a significant reduction in RV-C15-induced mRNA expression of *Il1b* and *Nlrp3,* demonstrating that TLR2 is required for RV-C15-mediated inflammasome priming (Fig 5D).

However, compared to RV-A1B-infected cells, levels of cleaved caspase-1 (caspase-1 p12), mature IL-1β, and secreted IL-1β were significantly decreased in RV-C15-infected THP-1 macrophages, indicating attenuated inflammasome activation (Fig 5B, 5C). To study virus entry, human THP-1-derived macrophages and mouse bone marrow-derived macrophages were incubated with RV-A1B or RV-C15 for 1 hour and washed three times with PBS. One hour after infection, RV-C15-infected human THP-1-derived macrophages and mouse bone marrow-derived macrophages showed reduced vRNA (Fig 5E) and vp3 levels (Fig 5F) compared to RV-A1B-infected cells. Consistent with this, confocal images of sham- and virus-infected THP-1 cells and primary mouse lung macrophages showed less viral entry into endosomes following infection with RV-C15 (Fig 5G). There was no mRNA expression of CDHR3 in either human THP-1 cells or mouse bone marrow macrophages (Fig 5H). Consistent with our previous study [34], there was no replication of RV-A1B in cultured macrophages (not shown). Together these data suggest that RV-C15-induced inflammasome activation is limited due to reduced entry of virions and viral genome.

Deficient inflammasome activation following RV-C15-infection in vivo.

We determined the effects of RV-C15 on inflammasome priming and activation in immature mice, comparing with RV-A1B. We collected lungs from RV-A1B- and RV-C15-infected six-day-old mice and measured inflammasome priming (pro-IL-1β and NLRP3) and inflammasome activation (IL-1β and caspase-1 p12). RV-C15 and RV-A1B induced an equal amount of pro-IL-1β and NLRP3 mRNA and protein expression one-day post-infection (Fig. 6A–6C), indicative of the equivalent inflammasome priming. However, cleavage of pro-IL-1β and caspase-1 and subsequent production of IL-1β and caspase-1 p12 was significantly attenuated in RV-C15-infected immature mice compared to RV-A1B (Fig. 6A, 6C).

We performed flow cytometry to determine the level of active caspase-1 and cellular source of IL-1β. Cells were stained with FLICA 660-YVAD-FMK reagent and fluorescent-tagged anti-pro-IL-1β, anti-CD45 and anti-F4/80. FLICA 660-YVAD-FMK is cell permeable and covalently binds with active caspase-1 enzyme. Compared to sham-infected six-day-old mice, both RV-A1B- and RV-C15-infected mice showed a greater percentage of pro-IL-1β+ lung cells and almost all of them were CD45+ F4/80+ (Fig. 6D), consistent with our previous finding that the airway macrophage is the major cellular source of IL-1β [31, 33]. There were no differences in these cell percentages with RV-A1B and RV-C15. On the contrary, the percentage of pro-IL-1β+ active caspase-1+ cells was significantly decreased in RV-C15-infected mice compared to RV-A1B (Fig. 6D).

IL-1β protects against RV-induced type 2 immune responses in vivo.

We previously showed in immature mice that inhibition of IL-1β responses with Anakinra increases RV-A1B-induced type 2 airway inflammation [31]. If reduced inflammasome activation and IL-1β production permit the exaggerated asthma phenotype associated with RV-C15 infection, then exogenous IL-1β should inhibit RV-C15-induced type 2 immune responses. We administered 0.1 ng of recombinant IL-1β intranasally to six-day-old mice 1 h prior to RV-C15 infection. Seven days after infection, mice treated with exogenous IL-1β showed decreased expression of *Il5* and *Il13* as well as mucus-related genes *Muc5ac, Muc5b* and *Clca1* (Fig. 7A). On the other hand, exogenous IL-1β had no effect on *Tnfa, Ifng, Cxcl1* or *Cxcl2* measured one-day post infection (Fig. 7B). IL-1β treatment had no significant effect on viral copy number one and four days post infection (Fig 7D). In addition, IL-1β inhibited lung IL-25 and IL-33 mRNA expression (Fig. 7C). Further, IL-1β attenuated RV-C15-induced airway responsiveness (Fig. 7E), mucus metaplasia (Fig. 7F and 7G), and lung ILC2s (Fig 7H).

Discussion

Early-life wheezing-associated respiratory infections with RV are associated with asthma development in high-risk infants [24–27] A multicenter prospective study of U.S. infants hospitalized for bronchiolitis found that infants with RV-C had a higher risk of physician-diagnosed asthma at 4 years of age [22]. We therefore compared the effects of RV-A1B infection and RV-C15 infection in immature mice. As we found previously, RV-A1B infection of six-day-old mice induced type 2 cytokine expression, mucous metaplasia,

airways hyperresponsiveness and ILC2 expansion. However, compared to RV-A1B, RV-C15 infection induced greater type 2 cytokine expression, mucous metaplasia, airway responsiveness and ILC2 expansion. Further, compared to RV-A1B, RV-C15-induced macrophage inflammasome activation was reduced *in vitro* and *in vivo.* Finally, treatment with IL-1β decreased RV-C15-induced type 2 cytokine and mucus-related gene expression, mucous metaplasia, airways responsiveness and ILC2 number, consistent with the notion that reduced inflammasome activation permits the asthma exaggerated phenotype. These data provide a mechanism by which early-life infection with RV-C could increase the risk of asthma later in life.

RV-C has been associated with severe respiratory illnesses in children and adults, including wheezing, O_2 supplementation, hospitalization and ICU admission. Infections with RV-C are more likely to occur in children with a history of asthma or who develop asthma [16–21]. Despite recognition of RV-C as a cause of severe exacerbation, virtually nothing is known about the pathogenesis of RV-C infections. RV-C has been refractory to study because it is difficult to grow *in vitro.* RV-C has been grown in primary mucociliary-differentiated human airway epithelial cells at air-liquid interface [35] and HeLa cells transduced with the CDHR3 AA allele (HeLa-E8 cells) [36]. An animal model of RV-C has not been established. To accomplish this, we infected six day-old mice with RV-C15 grown in HeLa-E8 cells overexpressing CDHR3 (from Y. Bochkov and J. Gern, University of Wisconsin). Lungs from RV-C15-infected mice showed significant increases in IFN-β mRNA expression, consistent with the presence of viral RNA. However, vRNA levels for both viruses peaked 24 h after inoculation, ruling out substantial replicative infection. To identify RV-C15, we used an antibody against EV-D68 vp3 which recognizes RV-A1B and RV-C15. RV-C15 localized to airway epithelial cells. As with RV-A1B, we also found examples of RV-C15 in airway macrophages.

Despite a similar amount of viral copies in the lung, RV-C15 infection of six day-old mice induced significantly higher levels of mRNA encoding the type 2 cytokines IL-5 and IL-13 than RV-A1B infection. Type 1 cytokines were not differentially expressed, however. mRNA expression of the IL-13-dependent mucus genes *Muc5ac, Muc5b* and *Clca1* was also significantly higher in RV-C15-infected mice. Accordingly, airways showed increased deposition of Muc5ac and more PAS-positive cells. Thus, infection of immature mice with RV-C15 induces an exaggerated mucous metaplasia phenotype compared to RV-A1B. Consistent with the production of IL-5 and IL-13 by ILC2s, we found more lineage-negative, ST2+ CD25+ CD127+ cells in the lungs of RV-C15-infected mice. Higher ILC2 numbers in RV-C15-infected mice were observed as early as four days after infection and maintained two weeks after infection. Our previous studies have shown that ILC2 expansion after early-life RV-A1B infection is driven by the innate cytokines IL-25, IL-33 and TSLP [28, 30]. We found that, compared to RV-A1B, RV-C15 infection of immature mice showed increased mRNA and protein abundance of these proteins, with deposition primarily in airway epithelial and subepithelial cells. Taken together, these data are consistent with human data showing that infants with severe RV bronchiolitis, who are more likely to have RV-C infection [21, 22], demonstrate higher nasopharyngeal levels of IL-5, IL-13 and TSLP. [23]

Macrophage inflammasome-mediated IL-1β limits RV-induced mucous metaplasia in immature mice by attenuating airway epithelial cell IL-25 and IL-33 expression. [31] We therefore reasoned that the higher level of innate cytokine expression in RV-C15-infected mice might be due, at least in part, to reduced inflammasome activation. In contrast to ICAM-1 and LDL family receptors, the receptors for major and minor group RVs, respectively, CDHR3 expression is restricted to ciliated airway epithelial cells. [13–15] Activation of the NLRP3 inflammasome requires at least two signals. Signal I, known as the priming signal, activates the NF-kB signaling pathway through activation by TNF-α or pattern recognition receptors such as the Toll-like receptors (TLRs) and Nod-like receptors, and induces expression of pro-IL-1β, pro-IL-18 and NLRP3 [37–39]. We found that RV-A and RV-C induced equal levels of inflammasome priming, and that priming by RV-C, as shown previously for RV-A [31, 33], was TLR2-dependent. The second step triggers oligomerization of NLRP3 and recruitment of the adaptor protein ASC and pro-caspase-1 to form an active inflammasome complex, leading to in turn to proteolytic cleavage of dormant pro-caspase-1 into active caspase-1 and conversion of the cytokine precursor pro-IL-1β into mature and biologically active IL-1β. Viral RNA is a potent stimulus of inflammasome activation [33, 40–42]. In the present study, RV-C15 inflammasome activation was decreased compared to RV-A1B both *in vitro* and *in vivo,* as evidenced by reduced protein abundance of cleaved caspase 1 and IL-1β, as well as fewer active lung caspase 1-containing CD45+F4/80+ cells. Compared to RV-A1B, there was less viral uptake of RV-C15 into cultured macrophages, as evidenced by decreased vRNA, vp3 and incorporation into late endosomes. CDHR3 was not expressed in cultured macrophages, consistent with the possibility that clathrin-mediated endocytosis is reduced in RV-C15-inoculated cells, thereby reducing the amount of intracellular viral genome available for NLRP3 inflammasome activation. In contrast, RV-C15-induced inflammasome priming likely rely on CDHR3- and clathrin-independent mechanisms of viral attachment and entry. For example, based on the atomic structure, sialic-acid-containing glycoproteins and gangliosides might act as attachment factors for RV-C15 [43], and studies in human airway epithelial cells suggest the existence of an RV-C co-receptor [15]. RV-C15 binding to a secondary, low affinity receptor may be sufficient for the initiation of signaling pathways required for inflammasome priming, but inadequate for inflammasome activation. In addition, macrophages employ clathrin-independent endocytic activities including flotillin-dependent endocytosis, caveolae-dependent endocytosis and macropinocytosis [44, 45].

To test whether inflammasome activation attenuates the viral-induced asthma phenotype, we treated mice with the inflammasome product IL-1β prior to RV-C15 infection. Treatment with IL-1β blocked lung expression of type 2 and innate cytokines (but not type 1 cytokines). These data are consistent with the notion that reduced inflammasome activation following RV-C15 infection permits the exaggerated asthma phenotype. On the other hand, it is also conceivable that RV-C15 directly stimulates increased innate cytokine expression by the airway epithelium, driving ILC2-dependent mucous metaplasia. Variances in the phosphorylation of kinases (p38, JNK, ERK5) and transcription factors (ATF-2, CREB, CEBPα) have been observed between major and minor group RVs [46] and it stands to reason that RV-C, which binds to a different receptor in the airway epithelium than major and minor group viruses, will elicit differential signaling and protein expression.

One weakness of this report is the lack of substantial viral replication in the mouse model. However, while replication of human RV is minimal in mice, we feel that the resulting host-induced innate immune response and immunopathology is still worthy of study. Our observation of different immune responses to RV-A1B, RV-C15 and enterovirus (EV)-D68 [47] which are qualitative in nature and resemble responses in human subjects suggest that the model is relevant to human disease. Another weakness is the absence of studies examining the identity of the RV-C receptor in mice. This will require the generation of a neutralizing antibody against mouse CDHR3.

We conclude that early-life RV-C infection induces an enhanced asthma phenotype in mice compared to RV-A. Macrophage NLRP3 inflammasome activation is reduced following RV-C infection, permitting exaggerated type 2 inflammation and mucous metaplasia.

Material and Methods

Ethics statement.

Mouse work was approved by the University of Michigan Animal Care and Use Committee, protocol # PRO00008264, and performed in according to the 2011 Guide for the Care and Use of Laboratory Animals.

Generation of RV-C15 and RV-A1B.

A cDNA infectious clone harboring the full-length RV-C15 genome and HeLa-E8 stable cells expressing human CDHR3 C529Y were provided by James Gern and Yury Bochkov, University of Wisconsin.[14] The cDNA was *in vitro* transcribed and resulting full-length vRNA transfected into HeLa-H1 cells (ATCC, Manassas, VA) using lipofectamine (ThermoFisher Scientific, Waltham, MA). Virus was harvested from the HeLa-H1 cell supernatants and used to infect HeLa-E8 cells. RV-A1B, RV-A2, RV-A16, HEV-D68 (ATCC, Manassas, VA) and RV-C15 were partially purified from infected HeLa cell lysates by ultrafiltration using a 100 kD cut-off filter [30]. Similarly concentrated and purified HeLa cell lysates were used for sham infection.

RV infection of mice.

Six day-old C57BL/6J mice (Jackson Laboratories, Bar Harbor, ME), male or female, were inoculated through the intranasal route under Forane anesthesia with 1.5×10^6 ePFU of RV-C15 in 15 μL PBS, 1.5×10^6 ePFU of RV-A1B in 15 μL PBS, or an equal volume of sham HeLa cell lysate. RV-C ePFU was calculated based on a calibrated standard curve for RV-A1B [43]. Littermates were randomly allocated to RV-C15, RV-A1B or sham treatment. Technicians were aware of the treatment allocation during the conduct of the experiments. Selected mice were treated intranasally with 0.1 ng of recombinant mouse IL-1β (R&D Systems, Minneapolis, MN), one hour before RV infection. Lungs were harvested 1, 2, 4, 7, 10, 14 or 21 days after infection for analysis.

Histology and immunofluorescence microscopy.

Three weeks after RV infection, lungs were perfused through the pulmonary artery with phosphate-buffered saline containing 5 mM EDTA. Next, lungs were inflated and fixed with

4% paraformaldehyde overnight. Five-micrometer–thick paraffin sections and processed for histology or fluorescence microscopy as described [30]. Lung sections were stained with PAS (Sigma-Aldrich, St Louis, MO) or Alexa Fluor 488-conjugated anti-Muc5ac at 1 μg/mL (Thermo Fisher Scientific, Rockford, IL) to visualize mucus. For RV-C staining, the presence of viral capsid protein was examined by Alexa Fluor 488-conjugated anti-HEV-D68 vp3 (GeneTex, Irvine, CA). This antibody recognizes vp3 from HEV-D68, RV-A1B, RV-A2, RV-A16 and RV-C15 (see online repository, Figure E1). Lung sections were incubated with anti-vp3, mouse anti-acetyl α-tubulin (MilliporeSigma, Burlington, MA), mouse anti-CD11b (Biolegend, San Diego, CA) and a rabbit polyclonal antibody raised against a conserved 14-amino acid sequence in the second calcium binding domain of human and mouse CDHR3 (produced by Genscript, Piscataway, NJ). For IL-25, IL-33 and TSLP staining, lung sections were harvested two days post-RV infection and stained with Alexa Fluor 488-conjugated rabbit anti-mouse IL-25/IL-17E (Millipore, Billerica, MA), Alexa Fluor 555-congjugated goat anti-mouse IL-33 (R&D Systems), and Alexa Fluor 555-congjugated rat anti-mouse TSLP (Biolegend). The level of PAS staining in the airway epithelium was quantified by NIH ImageJ software (Bethesda, MD). PAS and Muc5ac were represented as the fraction of PAS+ or Muc5ac+ epithelium compared with the total basement membrane length.

Flow cytometric analysis.

Lungs from sham-, RV-A1B-, and RV-C15-treated immature C57BL/6J mice were harvested one, four, seven, 10 or 14 days post-infection, perfused with PBS containing EDTA, minced, and digested in collagenase IV. Cells were filtered and washed with RBC lysis buffer, and dead cells were stained with PacBlue (Thermo Fisher Scientific). To identify ILC2s, cells were harvested 7 days post infection and then stained with fluorescent-tagged antibodies for lineage markers (CD3ε, TCRb, B220/CD45R,Ter-119, Gr-1/Ly-6G/Ly-6C, CD11b, CD11c, F4/80, and FcεRIa; all from BioLegend), anti-CD25 (BioLegend), anti-CD127 (eBioscience), and anti-ST2 (Biolegend) as described[28]. To determine caspase-1 activation, lung cells were harvested one-day post-infection and incubated with cell-permeable FLICA 660-YVAD-FMK caspase-1 inhibitor reagent (ImmunoChemistry Technologies, Bloomington, MN). Active caspase-1 enzyme covalently binds with FLICA 660-YVAD-FMK and retains the far-red fluorescent signal within the cell. Cells were then stained with fluorescent-tagged anti-CD45 and anti-F4/80 (BioLegend) and subsequently treated with permeabilization buffer (eBioscience) and stained with anti-IL-1β (eBioscience). Cells were detected using an LSR Fortessa Flow Cytometer (BD Biosciences, San Jose, CA). Data were collected using FACSDiva software (BD Biosciences) and analyzed using FlowJo software (TreeStar, Ashland, OR).

Quantitative real-time polymerase chain reaction (qPCR).

After solubilization with Trizol (Invitrogen), RNA was extracted from cells and tissue according to manufacturer's recommendations. Purified RNA was processed for first strand cDNA and qPCR using reverse transcriptase and SYBR green qPCR reagents (ThermoFisher Scientific). For *in vivo* experiments, mRNA *Il1b, Nlrp3, Tnf, Ifng, Cxcl1, Cxcl2, Il17* and *Il33* were measured 1 day post infection; *Ifna, Ifnb* and *Infl* mRNA was measured 2 days post infection and *Il5, Il25, Il13, Muc5ac,*

Muc5b and *Clca1* mRNA were measured 7 days post infection. Expression levels were normalized to GAPDH using the ΔΔCt method. Primers used are described in the online repository Table S1. To quantify virus particles, qPCR for positive-strand viral RNA was conducted using RV-specific primers and probes (forward primer: 5'-GTGAAGAGCCSCRTGTGCT-3'; reverse primer: 5'-GCTSCAGGGTTAAGGTTAGCC-3'; probe: 5'-FAM-TGAGTCCTCCGGCCCCTGAATG-TAMRA-3')[48].

Measurement of IL-1β, IL-25 and IL-33 protein levels.

Lung IL-25, IL-33 and TSLP (Thermo Fisher Scientific) were measured by ELISA. ELISA data were analyzed by BioTek Gen5 software (Winooski, VT). Total lung protein concentration was measured by BCA protein assay (Thermo Fisher Scientific).

Cell culture.

To generate bone marrow-derived macrophages, mouse bone marrow monocytes were isolated from C C57BL/6J and TLR2−/− (B6.129-Tlr2tm1Kir/J) mice (Jackson Laboratories) and cultured in L929 medium, a source of macrophage colony-stimulating factor, for 7 days [49]. Human primary peripheral blood mononuclear cells (PBMC; Precision for Medicine, Frederick, MD) were cultured in RPMI-1640 media supplemented with 20ng/mL of recombinant human M-CSF. THP-1 human monocytic cells (ATCC) were differentiated with 5 ng/ml of phorbol 12-myristate 13-acetate as described[50]. Cells were infected with RV-A1B and RV-C15 at a multiplicity of infection (MOI) of 1.0 at 33°C. To study virus entry, human THP-1-derived macrophages and mouse bone marrow-derived macrophages were incubated with RV-A1B or RV-C15 for 1 hour and washed three times with PBS. Viral RNA and CDHR3 mRNA expression were quantified by qPCR (see below) and the presence of RV-C was examined by Western blot and immunofluorescence using anti-EV-D68 vp3. Late endosomes were visualized with anti-EEA1 (Invitrogen, Carlsbad, CA). Images were visualized using a Leica SP5 inverted laser confocal microscope (Buffalo Grove, IL).

Western blot assay.

Lungs were harvested one day post-infection, dissolved in lysis buffer and homogenized for Western blot assay using anti-mouse IL-1β (R&D Systems), anti-mouse caspase-1 (Abcam, Cambridge, MA), anti-mouse NLRP3 (Cell Signaling Technology), and anti-β actin (Millipore Sigma, Burlington, MA). RV-A1B- and RV-C15-infected THP-1-derived macrophages were harvested one-day post-infection, dissolved in lysis buffer for Western blot assay using anti-human IL-1β (R&D Systems), anti-human caspase-1 (Abcam), anti-human NLRP3 (Abcam).

Assessment of airway responsiveness.

Airway responsiveness was assessed by measuring total respiratory system resistance after administration of nebulized saline and increasing doses of methacholine administered through an endotracheal tube [28, 32]. Due to the small size of the mice, these measurements were carried out four weeks after infection. Mechanical ventilation was conducted and

total respiratory system resistance measured using a Buxco FinePointe operating system (Wilmington, NC).

Quantification and statistical analysis.

Statistical analysis was performed using GraphPad Prism software (San Diego, CA). The number of animals per group was chosen as the minimum likely required for conclusions of biological significance, established from previous experience. A total of 272 mice were studied. No animals or data points were excluded from the analysis. Data are represented as mean ± standard error of the mean (SEM). For airways resistance data, statistical significance was assessed by two-way analysis of variance (ANOVA) with the two-stage linear step up procedure of Benjamini, Krieger and Yekutieli multiple comparisons test. For all other results, statistical significance was assessed by unpaired t-test or one-way analysis of variance (ANOVA), as appropriate. For one-way ANOVA, group differences were pinpointed by a Tukey multiple comparison test.

Supplementary Material

Refer to Web version on PubMed Central for supplementary material.

Acknowledgements

The authors thank James Gern and Yury Bochkov, University of Wisconsin School of Medicine and Public Health, for providing cDNA encoding RV-C15 and HeLa-E8 cells expressing CDHR3 C529Y.

Funding: This work was supported NIH grant R01 AI120526 and R01 AI155444 (to M.B. Hershenson)

References

1. Lau SKP, Yip CCY, Tsoi H-w, Lee RA, So L-y, Lau Y-l et al. Clinical features and complete genome characterization of a distinct human rhinovirus (HRV) genetic cluster, probably representing a previously undetected HRV Species, HRV-C, associated with acute respiratory illness in children. J Clin Microbiol 2007; 45(11): 3655–3664. [PubMed: 17804649]
2. Dominguez SR, Briese T, Palacios G, Hui J, Villari J, Kapoor V et al. Multiplex MassTag-PCR for respiratory pathogens in pediatric nasopharyngeal washes negative by conventional diagnostic testing shows a high prevalence of viruses belonging to a newly recognized rhinovirus clade. J Clin Virol 2008; 43(2): 219–222. [PubMed: 18674964]
3. Simmonds P, McIntyre C, Savolainen-Kopra C, Tapparel C, Mackay IM, Hovi T. Proposals for the classification of human rhinovirus species C into genotypically assigned types. J Gen Virol 2010; 91(10): 2409–2419. [PubMed: 20610666]
4. McIntyre CL, Knowles NJ, Simmonds P. Proposals for the classification of human rhinovirus species A, B and C into genotypically assigned types. J Gen Virol 2013; 94(8): 1791–1806. [PubMed: 23677786]
5. Bella J, Kolatkar PR, Marlor CW, Greve JM, Rossmann MG. The structure of the two amino-terminal domains of human ICAM-1 suggests how it functions as a rhinovirus receptor and as an LFA-1 integrin ligand. Proc Natl Acad Sci USA 1998; 95(8): 4140–4145. [PubMed: 9539703]
6. Vlasak M, Roivainen M, Reithmayer M, Goesler I, Laine P, Snyers L et al. The minor receptor group of human rhinovirus (HRV) includes HRV23 and HRV25, but the presence of a lysine in the VP1 HI loop is not sufficient for receptor binding. J Virol 2005; 79(12): 7389–7395. [PubMed: 15919894]

7. Gern JE, Galagan DM, Jarjour NN, Dick EC, Busse WW. Detection of rhinovirus RNA in lower airway cells during experimentally induced infection. Am J Respir Crit Care Med 1997; 155(3): 1159–1161. [PubMed: 9117003]
8. Johnston SL, Papi A, Bates PJ, Mastronarde JG, Monick MM, Hunninghake GW. Low grade rhinovirus infection induces a prolonged release of IL-8 in pulmonary epithelium. J Immunol 1998; 160(12): 6172–6181. [PubMed: 9637536]
9. Gern JE, Galagan DM, Dick EC. Rhinovirus enters but does not replicate inside airway macrophages. J Allergy Clin Immunol 1994; 93(1): 203–203.
10. Laza-Stanca V, Stanciu LA, Message SD, Edwards MR, Gern JE, Johnston SL. Rhinovirus replication in human macrophages induces NF-kappaB-dependent tumor necrosis factor alpha production. J Virol 2006; 80(16): 8248–8258. [PubMed: 16873280]
11. Hosoda M, Yamaya M, Suzuki T, Yamada N, Kamanaka M, Sekizawa K et al. Effects of rhinovirus infection on histamine and cytokine production by cell lines from human mast cells and basophils. J Immunol 2002; 169(3): 1482–1491. [PubMed: 12133975]
12. Akoto C, Davies DE, Swindle EJ. Mast cells are permissive for rhinovirus replication: potential implications for asthma exacerbations. Clin Exp Allergy 2017; 47(3): 351–360. [PubMed: 28008678]
13. Griggs TF, Bochkov YA, Basnet S, Pasic TR, Brockman-Schneider RA, Palmenberg AC et al. Rhinovirus C targets ciliated airway epithelial cells. Respir Res 2017; 18(1): 84. [PubMed: 28472984]
14. Bochkov YA, Watters K, Ashraf S, Griggs TF, Devries MK, Jackson DJ et al. Cadherin-related family member 3, a childhood asthma susceptibility gene product, mediates rhinovirus C binding and replication. Proc Natl Acad Sci USA 2015; 112(17): 5485–5490. [PubMed: 25848009]
15. Everman JL, Sajuthi S, Saef B, Rios C, Stoner AM, Numata M et al. Functional genomics of CDHR3 confirms its role in HRV-C infection and childhood asthma exacerbations. J Allergy Clin Immunol 2019. 144(4):962–971. [PubMed: 30930175]
16. Miller EK, Edwards KM, Weinberg GA, Iwane MK, Griffin MR, Hall CB et al. A novel group of rhinoviruses is associated with asthma hospitalizations. J Allergy Clin Immunol 2009; 123(1): 98–104.e101. [PubMed: 19027147]
17. Bizzintino J, Lee W-M, Laing IA, Vang F, Pappas T, Zhang G et al. Association between human rhinovirus C and severity of acute asthma in children. Eur Respir J 2011; 37(5): 1037–1042. [PubMed: 20693244]
18. Cox DW, Bizzintino J, Ferrari G, Khoo SK, Zhang G, Whelan S et al. Human rhinovirus species C infection in young children with acute wheeze is associated with increased acute respiratory hospital admissions. Am J Respir Crit Care Medicine 2013; 188(11): 1358–1364.
19. Moreno-Valencia Y, Hernandez-Hernandez VA, Romero-Espinoza JAI, Coronel-Tellez RH, Castillejos-Lopez M, Hernandez A et al. Detection and characterization of respiratory viruses causing acute respiratory illness and asthma exacerbation in children during three different seasons (2011–2014) in Mexico City. Influenza Other RespirViruses 2015; 9(6): 287–292.
20. Fawkner-Corbett DW, Khoo SK, Duarte CM, Bezerra PGM, Bochkov YA, Gern JE et al. Rhinovirus-C detection in children presenting with acute respiratory infection to hospital in Brazil. J Med Virol 2016; 88(1): 58–63. [PubMed: 26100591]
21. Cox DW, Khoo S-K, Zhang G, Lindsay K, Keil AD, Knight G et al. Rhinovirus is the most common virus and rhinovirus-C is the most common species in paediatric intensive care respiratory admissions. Eur Respir J 2018; 52(2).
22. Hasegawa K, Mansbach JM, Bochkov YA, Gern JE, Piedra PA, Bauer CS et al. Association of rhinovirus C bronchiolitis and immunoglobulin E sensitization during infancy with development of recurrent wheeze. JAMA Pediatrics 2019; 173(6): 544–552. [PubMed: 30933255]
23. Hasegawa K, Hoptay CE, Harmon B, Celedón JC, Mansbach JM, Piedra PA et al. Association of type 2 cytokines in severe rhinovirus bronchiolitis during infancy with risk of developing asthma: A multicenter prospective study. Allergy; 2019;74:1374–1377. [PubMed: 30656708]
24. Rubner FJ, Jackson DJ, Evans MD, Gangnon RE, Tisler CJ, Pappas TE et al. Early life rhinovirus wheezing, allergic sensitization, and asthma risk at adolescence. J Allergy Clin Immunol 2017; 139(2): 501–507. [PubMed: 27312820]

25. van Meel ER, den Dekker HT, Elbert NJ, Jansen PW, Moll HA, Reiss IK et al. A population-based prospective cohort study examining the influence of early-life respiratory tract infections on school-age lung function and asthma. Thorax 2018; 73(2): 167–173. [PubMed: 29101282]
26. Moraes TJ, Sears MR. Lower respiratory infections in early life are linked to later asthma. Thorax 2018; 73(2): 105–106. [PubMed: 29170249]
27. Martorano LM, Grayson MH. Respiratory viral infections and atopic development: From possible mechanisms to advances in treatment. Eur J Immunol 2018; 48(3): 407–414. [PubMed: 29244204]
28. Hong JY, Bentley JK, Chung Y, Lei J, Steenrod JM, Chen Q et al. Neonatal rhinovirus induces mucous metaplasia and airways hyperresponsiveness through IL-25 and type 2 innate lymphoid cells. J Allergy Clin Immunol 2014; 134(2): 429–439. [PubMed: 24910174]
29. Rajput C, Cui T, Han M, Lei J, Hinde JL, Wu Q et al. RORα-dependent type 2 innate lymphoid cells are required and sufficient for mucous metaplasia in immature mice. Am J Physiol: Lung Cell Mol Physiol 2017; 312(6): L983–L993. [PubMed: 28360114]
30. Han M, Rajput C, Hong JY, Lei J, Hinde JL, Wu Q et al. The innate cytokines IL-25, IL-33, and TSLP cooperate in the induction of type 2 innate lymphoid cell expansion and mucous metaplasia in rhinovirus-infected immature mice. J Immunol 2017; 199(4): 1308–1318. [PubMed: 28701507]
31. Han M, Ishikawa T, Bermick JR, Rajput C, Lei J, Goldsmith AM et al. IL-1β prevents ILC2 expansion, type 2 cytokine secretion, and mucus metaplasia in response to early-life rhinovirus infection in mice. Allergy 2020; 2020;75:2005–2019
32. Schneider D, Hong JY, Popova AP, Bowman ER, Linn MJ, McLean AM et al. Neonatal rhinovirus infection induces persistent mucous metaplasia and airways hyperresponsiveness J Immunol 2012; 188: 2894–2904. [PubMed: 22331068]
33. Han M, Bentley JK, Rajput C, Lei J, Ishikawa T, Jarman CR et al. Inflammasome activation is required for human rhinovirus-induced airway inflammation in naïve and allergen-sensitized mice. Mucosal Immunol 2019. 12 (4), 958–968 [PubMed: 31089187]
34. Saba TG, Chung Y, Hong JY, Sajjan US, Bentley JK, Hershenson MB. Rhinovirus-induced macrophage cytokine expression does not require endocytosis or replication. Am J Respir Cell Mol Biol 2014; 50(5): 974–984. [PubMed: 24783958]
35. Ashraf S, Brockman-Schneider R, Gern JE. Propagation of rhinovirus-C strains in human airway epithelial cells differentiated at air-liquid interface. In: Jans DA, Ghildyal R (eds). Rhinoviruses: Methods and Protocols. Springer New York: New York, NY, 2015, pp 63–70.
36. Bochkov YA, Watters K, Basnet S, Sijapati S, Hill M, Palmenberg AC et al. Mutations in VP1 and 3A proteins improve binding and replication of rhinovirus C15 in HeLa-E8 cells. Virology 2016; 499: 350–360. [PubMed: 27743961]
37. Franchi L, Eigenbrod T, Núñez G. Cutting Edge: TNF-α Mediates Sensitization to ATP and Silica via the NLRP3 Inflammasome in the Absence of Microbial Stimulation. J Immunol 2009; 183(2): 792–796. [PubMed: 19542372]
38. Bauernfeind FG, Horvath G, Stutz A, Alnemri ES, MacDonald K, Speert D et al. Cutting edge: NF-kappaB activating pattern recognition and cytokine receptors license NLRP3 inflammasome activation by regulating NLRP3 expression. J Immunol2009; 183(2): 787–791. [PubMed: 19570822]
39. He Y, Hara H, Nunez G. Mechanism and regulation of NLRP3 inflammasome activation. Trends Biochem Sci 2016; 41(12): 1012–1021. [PubMed: 27669650]
40. Rajan JV, Warren SE, Miao EA, Aderem A. Activation of the NLRP3 inflammasome by intracellular poly I:C. 2010; 584(22): 4627–4632.
41. Franchi L, Eigenbrod T, Muñoz-Planillo R, Ozkurede U, Kim Y-G, Chakrabarti A et al. Cytosolic double-stranded RNA activates the NLRP3 inflammasome via MAVS-induced membrane permeabilization and K+ efflux. J Immunol 2014; 193(8): 4214–4222. [PubMed: 25225670]
42. Li J, Hu L, Liu Y, Huang L, Mu Y, Cai X et al. DDX19A senses viral RNA and mediates NLRP3-dependent inflammasome activation. J Immunol 2015; 195(12): 5732–5749. [PubMed: 26538395]
43. Liu Y, Hill MG, Klose T, Chen Z, Watters K, Bochkov YA et al. Atomic structure of a rhinovirus C, a virus species linked to severe childhood asthma. Proc Natl Acad Sci USA 2016; 113(32): 8997–9002. [PubMed: 27511920]

44. Mercer J, Greber UF. Virus interactions with endocytic pathways in macrophages and dendritic cells. Trends Microbiol 2013; 21(8): 380–388. [PubMed: 23830563]

45. Nikitina E, Larionova I, Choinzonov E, Kzhyshkowska J. Monocytes and macrophages as viral targets and reservoirs. Int J Mol Sci; 19(9).

46. Schuler BA, Schreiber MT, Li L, Mokry M, Kingdon ML, Raugi DN et al. Major and minor group rhinoviruses elicit differential signaling and cytokine responses as a function of receptor-mediated signal transduction. PLoS One 2014; 9:e93897. [PubMed: 24736642]

47. Rajput C, Han M, J.K. B, Lei J, Ishikawa T, Wu Q et al. Enterovirus D68 infection induces IL-17-dependent neutrophilic airway inflammation and hyperresponsiveness. JCI Insight 2018.

48. Contoli M, Message SD, Laza-Stanca V, Edwards MR, Wark PA, Bartlett NW et al. Role of deficient type III interferon-lambda production in asthma exacerbations. Nat Med 2006; 12: 1023–1026. [PubMed: 16906156]

49. Han M, Chung Y, Hong JY, Rajput C, Lei J, Hinde JL et al. Toll-like receptor 2-expressing macrophages are required and sufficient for rhinovirus-induced airway inflammation. J Allergy Clin Immunol 2016; 138(6): 1619–1630. [PubMed: 27084403]

50. Park EK, Jung HS, Yang HI, Yoo MC, Kim C, Kim KS. Optimized THP-1 differentiation is required for the detection of responses to weak stimuli. Inflammation Res 2007; 56(1): 45–50.

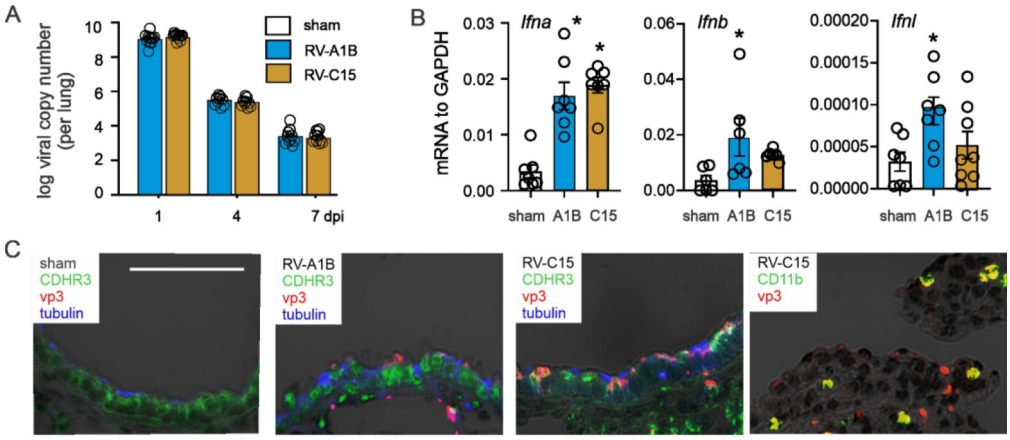

FIG 1. Infection of six-day-old mice with RV-C15.

A, RV positive-strand RNA was assessed 1, 4 and 7 days after infection, and presented as viral copy number in total lung (N = 9–12, from three experiments, mean±SEM). ***B***, Lung mRNA expression of *Ifna, Ifnb* and *Ifnl* measured 2 d post infection (N = 7 from two experiments, mean±SEM, *different from sham, one-way ANOVA). ***C***, Two days after infection, airways from RV-C15-infected mice were stained with anti-VP3 (red), anti-acetyl α-tubulin (blue), anti-CDHR3 or CD11b (green). Acetyl α-tubulin was localized to the epithelial cell apical surface. RV-C15 co-localized with CDHR3 in ciliated airway epithelial cells and CD11b in airway macrophages. Scale bar, 50 μm.

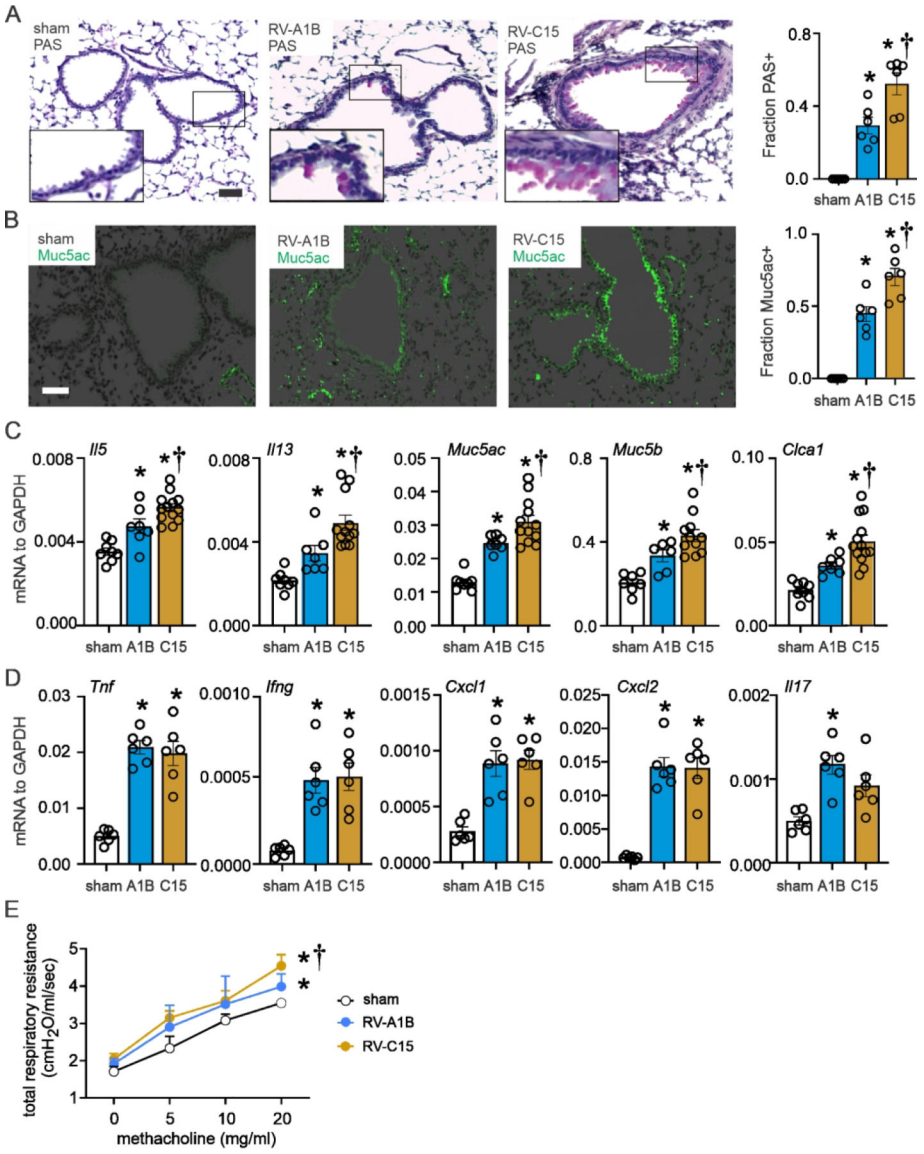

FIG 2. RV-C15 exaggerates the development of an asthma like phenotype and type 2 responses in immature mice.

6-day old wild type C57BL/6 mice were inoculated with sham, RV-A1B, or RV-C15. Mucous metaplasia was assessed by PAS staining (***A***) and Muc5ac immunofluorescence (***B***). Lung sections prepared 3 wk after treatment of 6-d-old mice. ***C*** and ***D***. Lung mRNA expression of *Il5, Il13, Muc5ac, Muc5b,* and *Clca1* (measured 7 d post infection) and *Tnf, Ifng, Cxcl1, Cxcl2,* and *Il17* (measured 1 d post infection) (n = 6–13 from two experiments, mean±SEM, *different from sham, †different from RV-A1B, p<0.05, one-way ANOVA). ***E***. Airway saline and methacholine responsiveness was measured three weeks post-infection (N = 3–4, mean ± SEM, *different from sham, †different from RV-A1B, p < 0.05, two-way ANOVA with two-stage linear step up procedure of Benjamini, Krieger and Yekutieli multiple comparisons test).

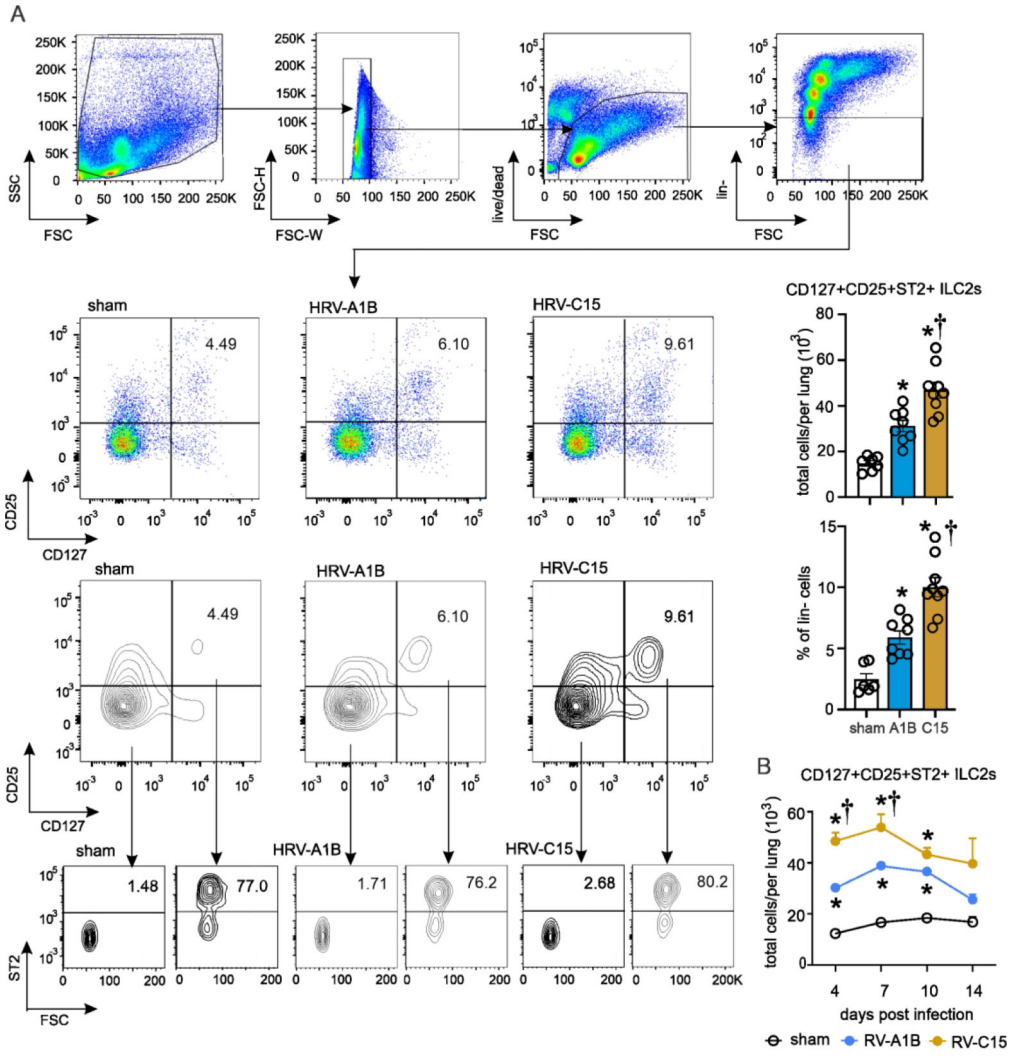

FIG 3. Lung lineage-negative CD25$^+$ CD127$^+$ ST2$^+$ ILC2s in RV-infected six-day-old mice.

(***A*** and ***B***) 6-day old wild type C57BL/6 mice were inoculated with sham, RV-A1B, or RV-C15. Four, 7, 10 or 14 days later, live ILC2s were identified as lineage-negative (upper panels), CD25+ CD127+ (middle panels, both dot plot and contour plots are shown) and ST2+ (lower panels). (***B***) ILC2s were quantified as a percentage of lin-cells and as a total ILC2s per lung (n = 6–9, mean±SEM from two experiments for day 7; n = 3–4, mean±SEM from one experiment for days 4, 10 and 14, *different from sham, †different from RV-A1B, $p<0.05$, one-way ANOVA).

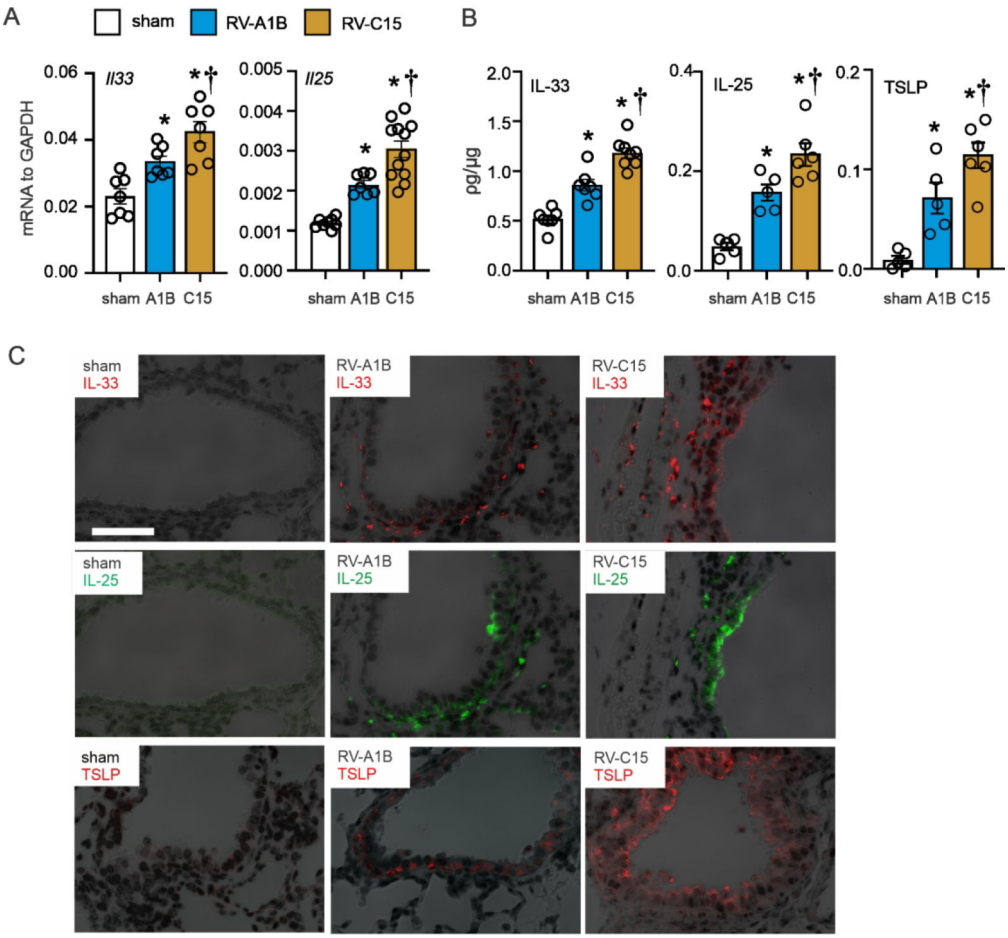

FIG 4. Innate cytokine expression in RV-infected six-day-old mice.

6-day old C57BL/6 mice were inoculated with sham, RV-A1B, and RV-C15. Whole-lung mRNA (***A***) was measured using quantitative PCR, and whole lung IL-33, IL-25, and TSLP protein (***B***) were examined by ELISA. (N = 7–12 from two experiments, mean±SEM, *different from sham, †different from RV-A1B, $p<0.05$, one-way ANOVA). ***C,*** Two days post-infection, lungs were stained for IL-33 (red), IL-25 (green), TSLP (red) and nuclei (DAPI, black). Scale bar, 50 μM.

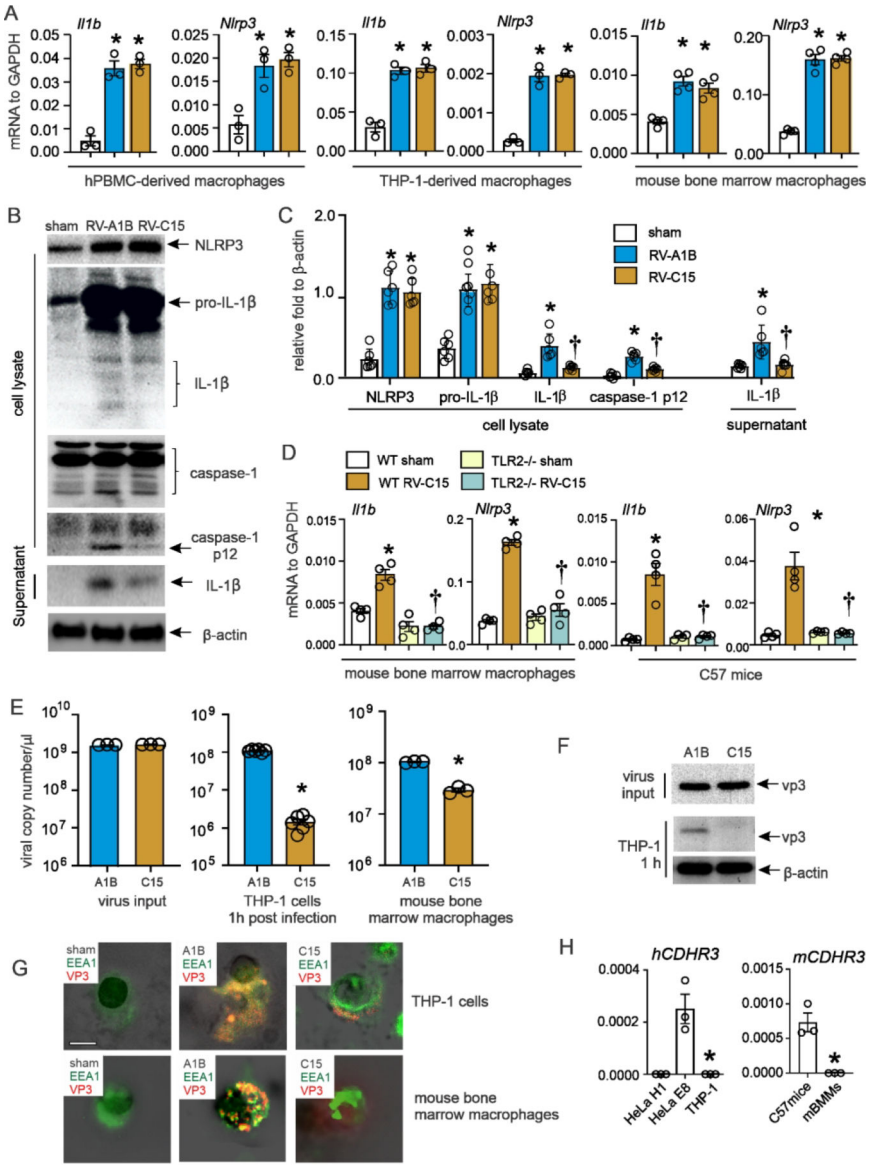

FIG 5. Inflammasome activation in RV-C15-infected macrophages.

A, human PBMC macrophages, human THP-1 macrophages, and mouse bone marrow-derived macrophages were infected with sham, RV-A1B, or RV-C15 at an MOI of 1 for 24 hours. Cell lysate was harvested for mRNA expression. ***B,*** both cell lysate and supernatant from RV-infected human THP-1 macrophages were collected for immunoblot assay. Anti-human-IL-1β recognizes pro-IL-1β and its bioactive form IL-1β. Anti-human-caspase-1 detects both caspase-1 and its cleaved form, caspase-1 p12. ***C,*** group mean relative expression levels were normalized to β-actin. (N= 6 from five individual experiments, mean±SEM, *different from sham, †different from RV-A1B, $p<0.05$, one-way ANOVA.) ***D,*** mouse bone marrow-derived macrophages isolated from both WT and TLR2−/− mice were infected with sham or RV-C15. Lung or cells were harvested 24 hours post infection for mRNA. ***E-F*** human THP-1 macrophages and mouse bone marrow-derived macrophages were incubated with RV-A1B or RV-C15 at an MOI of 1 for 1 hour at 33°C and

subsequently washed three times with PBS. RV positive strand RNA (**E**) was assessed 1, 6, 16, 24, 36, or 48 hours after infection, and presented as viral copy number per μl of RNA. (N =3–6, mean±SEM, * different from RV, $p<0.05$, unpaired t-test). The viral protein (**F**) was examined by Western blot using anti-vp3 antibody. ***G,*** Human THP-1 cells (upper panel) and mouse bone marrow derived macrophages (lower panel) were incubated with RV-A1B and RV-C at an MOI of 1for 1 hour at 33°C and subsequently stained for vp3 (red), EEA1 (green), and nuclei (DAPI, black). ***H,*** CDHR3 mRNA expression in human THP-1 cells and mouse bone marrow-derived macrophages.

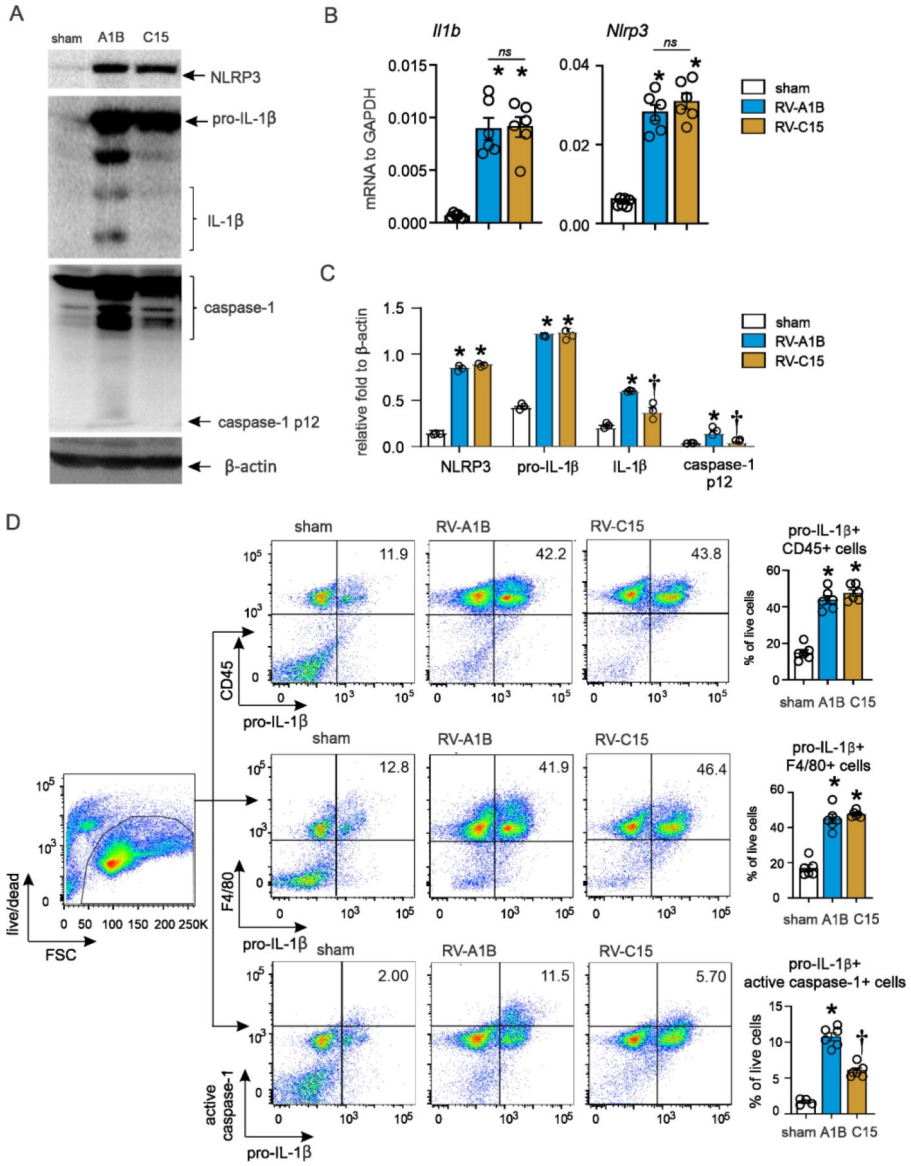

FIG 6. Deficient inflammasome activation in RV-C15-infected immature mice.

6-day old C57BL/6 mice were inoculated with sham, RV-A1B, or RV-C15. ***A,*** one day after infection, whole lungs were homogenized within the lysis buffer and subjected to Western blot. Anti-mouse-IL-1β recognizes pro-IL-1β and its bioactive form IL-1β. Anti-mouse-caspase-1 detects both caspase-1 and its cleaved form, caspase-1 p12. ***B,*** Group mean relative expression levels were normalized to β-actin. (N=3 from three experiments, mean±SEM, *different from sham, †different from RV-A1B, $p<0.05$, one-way ANOVA.) ***C,*** mRNA expression was measured 1day later. (N=6 from two experiments, mean±SEM, *different from sham, $p<0.05$, one-way ANOVA with Tukey's multiple comparisons test.) ***D,*** lung pro-IL-1β+ cells in RV-infected six-day-old mice. Pro-IL-1β+ cells were identified 1 d after infection. Pro-IL-1β+/CD45+, pro-IL-1β+/F4/80+, and pro-IL-1β+/ active caspasae-1+ cells were analyzed as a percentage of live cells, respectively (n = 4, mean±SEM, *different from sham, †different from RV-A1B, $p<0.05$, one-way ANOVA).

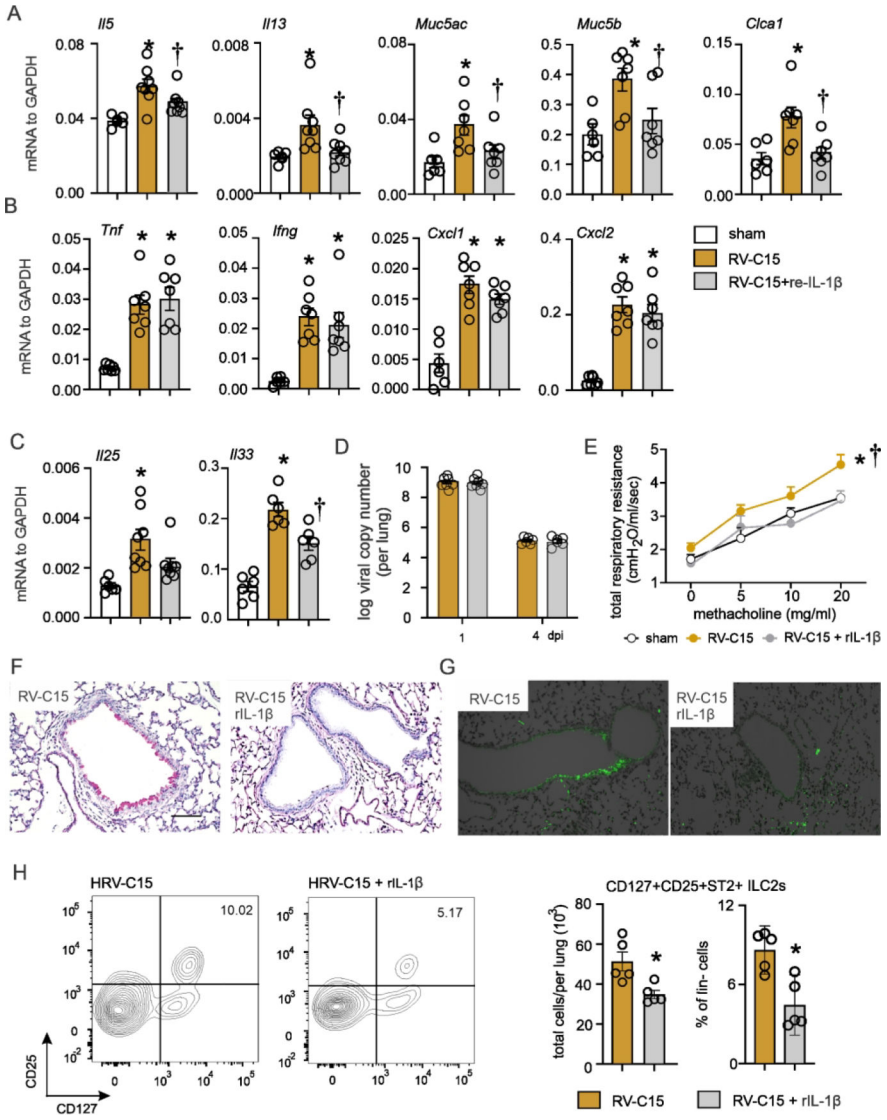

FIG 7. IL-1β treatment is protective against RV-C15-induced type 2 inflammation.

Six-day-old C57BL/6 mice were inoculated with sham or RV in combination with recombinant mouse IL-1β (rIL-1β) ***A-C.*** Whole-lung mRNA and protein were assessed 1 day *(Tnf, Cxcl1, Cxcl2, Ifng and Il33)* or 7 days *(Il5, Il13, Il25, Muc5ac, Muc5b* and *Clca1)* post infection. (N = 6–8 from two experiments, mean±SEM, *different from sham, $p<0.05$; † different from RV-C15, $p<0.05$, one-way ANOVA). ***D.*** RV positive strand RNA was assessed one and four days after infection and presented as viral copy number in total lung. (N =6–7 from two experiments, mean±SEM, *different from sham, $p<0.05$; † different from RV-C15, $p<0.05$, one-way ANOVA). ***E.*** Airway methacholine responsiveness was measured three weeks post-infection. (N = 3–4, mean ± SEM, *different from sham, †different from RV-C15 + rIL-1β, $p < 0.05$, two-way ANOVA with two-stage linear step up procedure of Benjamini, Krieger and Yekutieli multiple comparisons test. Note: data shown for sham and RV-C are identical to those in Figure 2. Airway resistance results were separated into two figures for clarity.) ***F*** and ***G***. Mucous metaplasia was assessed by PAS staining (F) and

Muc5ac immunofluorescence (G). Lung sections prepared 3 wk after treatment of 6-day-old mice. ***H.*** 6-day old wild type C57BL/6 mice were inoculated with RV-C15 and recombinant IL-1β. Seven days later, live ILC2s were identified as lineage-negative, CD25+, CD127+ and ST2+ cells (panel shows only CD25 and CD127 for clarity). ILC2s were quantified as total ILC2s per lung and percent of lineage-negative cells (n =5, mean±SEM from one experiment, *different from RV-C15, $p<0.05$, unpaired t-test).